ACS Photonics

Letter

pubs.acs.org/journal/apchd5

Near-Field Mapping of Optical Modes on All-Dielectric Silicon Nanodisks

Terefe Getaneh Habteyes,*[,†,‡] Isabelle Staude,*[,†,§] Katie E. Chong,[§] Jason Dominguez,[⊥] Manuel Decker,[§] Andrey Miroshnichenko,[§] Yuri Kivshar,[§] and Igal Brener[⊥]

[‡]Department of Chemistry and Chemical Biology, and Center for High Technology Materials, University of New Mexico, Albuquerque, New Mexico 87131, United States

[§]Nonlinear Physics Centre, Research School of Physics and Engineering, The Australian National University, Canberra, ACT 0200, Australia

[⊥]Center for Integrated Nanotechnologies, Sandia National Laboratories, Albuquerque, New Mexico 87185, United States

Supporting Information

ABSTRACT: We measure, for the first time to our knowledge, the near-field amplitudes and phases of localized optical modes of high-index all-dielectric nanoparticles using apertureless near-field optical microscopy. For individual silicon nanodisks, we observe a four-lobed mode pattern and the formation of deep-subwavelength hot-spots. Our numerical calculations of the optical near-fields of the nanodisks in combination with a multipole expansion of the scattered field based on vector spherical harmonics reveal that the observed modes are dominated by electric quadrupole contributions. The observed mode is of particular interest for the design of low-loss all-dielectric metasurfaces and nanoantennas for a broad range of applications, such as directional and complex-polarization controlled emission, light extraction from multipolar atomic transitions, and coherent multiple-emitter-nanocavity interactions.

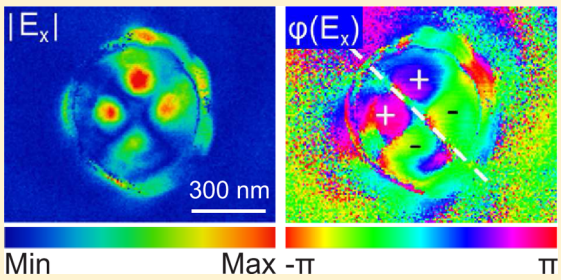

KEYWORDS: *near-field microscopy, all-dielectric nanophotonics, subwavelength structures, nanostructures, quadrupole mode*

Owing to their low dissipative losses, high-permittivity all-dielectric nanoparticles are emerging as a promising alternative to metallic nanoparticles for a wide range of nanophotonic applications that utilize localized resonant modes.[1] This development is fuelled by recent experimental studies revealing strong magnetic response even for simple nanoparticle shapes.[2−7] The very low losses in combination with the multipolar characteristics of both the electric and the magnetic optical modes supported by such nanoparticles offer unique opportunities for the design of metasurfaces and optical nanoantennas. For example, controlled interference of electric and magnetic resonances with defined multipolar character is key for tailoring directional scattering from all-dielectric nanoparticles.[5,6,8,9] As another example, the very low dissipative losses of the constituent dielectric materials allows the observation of potentially very sharp Fano-resonances in composite all-dielectric nanoparticles;[10,11] sharp resonances usually translate into better sensitivity for chemical and biosensors. Much of the recent research in this field has been focused on the study of the optical properties of such high-permittivity all-dielectric nanoparticles, with experiments reporting almost exclusively far-field measurements.[2−7] However, standard far-field measurements provide only very limited information about the multipolar character of higher order optical modes. The use of these higher-order multipolar modes offers new opportunities for directional[12] and complex-polarization controlled[13] emission from nanoemitters. Furthermore, these modes could allow for targeted near-field coupling to higher-order optical transitions of molecules or doped nanocrystals or even for coherent nanoparticle-mediated interactions between multiple nanoemitters.[14]

Cathodoluminescence imaging spectroscopy of the near fields of resonant modes supported by single silicon cylinders has been performed recently.[15] However, the employed excitation via an electron beam does not provide direct control over the polarization of the excited mode, nor does it allow to obtain information about the local phase of its optical near-fields.

Here, for the first time to our knowledge, we perform all-optical near-field imaging with a spatial resolution on the order of 10 nm[16] of localized modes of individual high-index all-dielectric nanoparticles (silicon nanodisks) using apertureless (scattering type) near-field scanning optical microscopy (ANSOM). A sketch of the measurement setup is shown in Figure 1. The basic principle of ANSOM imaging involves focusing an external laser light at the tip of an atomic force microscope probe and measuring the scattered light as the sample is raster scanned in close proximity to the tip.[17,18] ANSOM has been used to image the near-field characteristics

Received: June 27, 2014
Published: August 18, 2014

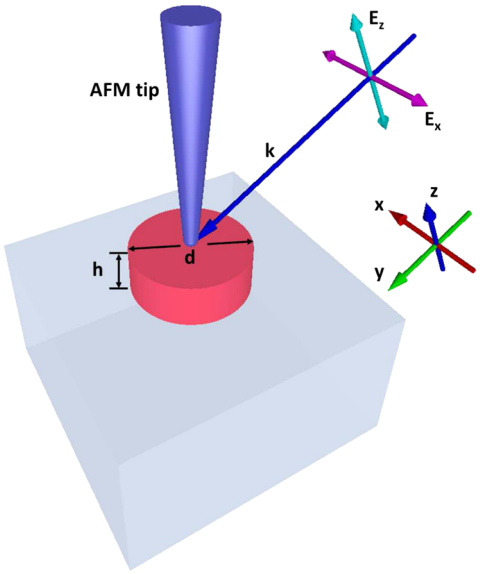

Figure 1. Schematic of the tip of the atomic force microscope probe on a silicon disk of height h = 140 nm and diameter d = 412 nm on a silicon-on-insulator wafer during the measurement process. A laser beam (633 nm wavelength) is focused onto the tip with an NA = 0.46 parabolic mirror. The central ray is incident with a wavevector k oriented at an angle of 60° with respect to the sample surface normal. Also shown are the directions of the electric field components E_x and E_z. The incident beam is x-polarized. The polarization of the detected scattered electric field is selected interferometrically, such that the polarization of the detected light is determined by the polarization of the reference beam.

of materials with spatial resolution independent of the wavelength of light.[19] In particular, it has provided remarkably high-resolution maps of plasmonic near-fields.[20−24] ANSOM has also been used to map dielectric contrast and dielectric/semiconductor nanoparticles before.[25−28] However, resolving the near-field profiles of particular localized modes of high-index all-dielectric nanoparticles has never been attempted so far. Despite having proven a powerful tool for mapping the near-field profiles of plasmonic nanoparticles in the past, the applicability of ANSOM techniques for all-dielectric nanoparticles cannot be taken for granted due to the fundamental physical differences of the localized excitations supported by high-index all-dielectric nanoparticles as compared to plasmonic systems. Most importantly, the optical modes of the high-index dielectric nanoparticles originate from the excitation of optically induced displacement currents instead of ohmic currents. Furthermore, while for plasmonic nanoparticles the fields are mainly concentrated at the metal surface, in the case of all-dielectric nanoparticles, they penetrate the entire particle and the field maxima are usually formed inside the nanoparticles. This results in an experimental challenge to map low field enhancement on the surface as the sensitivity of the probe to the subphase field decreases with distance away from the tip. Additional technical challenges arise from narrower resonance widths (higher Q-factors), which originate from the lower losses of all-dielectric structures in comparison to plasmonic structures.

Silicon nanodisks on a silicon oxide layer were fabricated using electron-beam lithography on silicon-on-insulator (SOI) wafers. The top-silicon thickness was first reduced to 140 nm, followed by the lithography steps and then directional reactive ion etching. The details of the fabrication process can be found in the Methods section. The fabricated silicon nandisks have a height of 140 nm and top-view diameters of around 450 nm. Due to a slight negative side-wall-inclination of ∼15° for the employed etching procedure, the effective optical diameters of the silicon nanoparticles are a few tens of nanometers smaller. The center-to-center spacing between adjacent nanodisks is set to 2 μm in order to minimize mutual coupling (see Figures 2a

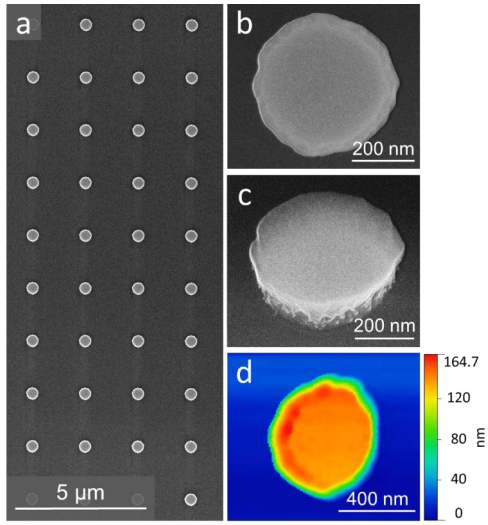

Figure 2. (a) Scanning electron micrograph of a typical fabricated silicon nanodisk sample. (b, c) Magnified and oblique views of a single nanodisk, respectively. (d) Topography of a single nanodisk recorded using the atomic-force microscopy functionality of the ANSOM.

and S1). Scanning electron micrographs of a typical fabricated sample are displayed in Figure 2. Based on numerical predictions, the dimensions of the fabricated silicon nanodisks were chosen to allow for excitation of the quadrupole mode at 60° tilted incidence at 633 nm wavelength. In experiment, geometric tuning of the actual quadrupole resonance frequency to the fixed laser wavelength of 633 nm has been realized via a slight variation of the nanodisk diameters of several tens of nanometers. Note that the fundamental electric and magnetic dipole modes of all fabricated structures will appear in the near-infrared spectral range.

Polarization selective ANSOM imaging has been performed by configuring the optical components around a Neaspec atomic force microscope (AFM) customized for pseudoheterodyne interferometric detection of scattered light (see Methods for details). A linearly x-polarized laser beam is focused at the probe tip at a 60° angle with respect to the surface normal as shown in Figure 1. The collected scattered light is mixed with a reference beam and detected using a silicon photodiode. The output of the detector is demodulated at 4Ω, where $\Omega \approx 250$ kHz is the resonance oscillation frequency of the cantilever. The images for the measured in-plane (E_x) and out-of-plane (E_z) optical near-field amplitudes and phases of a single nanodisk in the array with nanodisk dimensions providing the strongest resonant quadrupolar response in near-field experiments are shown in Figure 3a−d. The scanned area was 1.1 μm × 0.87 μm.

For both polarization schemes, the near-field distribution of the individual silicon nanodisks has four prominent lobes, as seen in the amplitude as well as in the phase images. Note that each of the lobes features a deep-subwavelength hot spot of around 60 nm in diameter at the nanodisk surface (see Figure

dx.doi.org/10.1021/ph500232u | ACS Photonics 2014, 1, 794−798

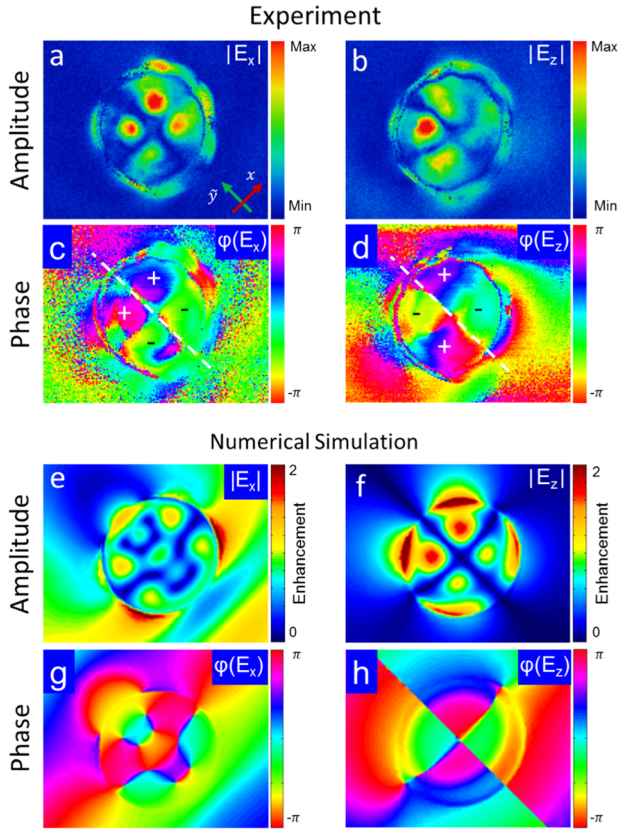

Figure 3. (a–d) Experimentally measured optical near-field amplitude (a, b) and phase (c, d) profiles of a single silicon nanodisk demodulated at 4× (4Ω) the cantilever oscillation frequency for (a, c) *x*- and (b, d) *z*-polarization. The arrows in (a) denote the *x*-direction and the projection of the *y*-direction onto the sample plane. (e–h) Corresponding simulated electric near-field enhancement (e, f) and phase profiles (g, h) 1 nm above the disk surface. The four lobes in each of the images as well as the symmetry properties of their phase characteristics with respect to the white dashed lines in (c, d) show good agreement with experimental data.

3a,b), which corresponds to less than one-tenth of the free space wavelength and less than a third of the wavelength of light in silicon. As such, our measurements provide direct evidence that high-index all-dielectric nanoparticles, similar to plasmonic particles, have the ability to confine light to deep-subwavelength dimensions. Notably, while the measured amplitudes look similar for both polarization schemes, the phase images reveal even/odd symmetry with respect to a common axis (dashed lines in Figure 3c,d) for *x*- and *z*-polarization, respectively. Additional measurements of E_x for samples with an about 5 nm smaller nanodisk radius are included in the Supporting Information, demonstrating the reproducibility and robustness of our findings (see Figure S1).

To compare our experimental results with theory we performed numerical simulations using CST Microwave Studio with a nanodisk diameter of 412 nm and a nanodisk height of 140 nm. Note that the choice of the diameter takes the slightly trapezoidal shape of the fabricated silicon nanoparticles into account. The substrate has been neglected for simplicity. We extract the near-field enhancement in a plane 1 nm above the nanodisk surface. These results are shown in Figure 3e–h for the respective field components relevant for the two polarization schemes. A very good overall agreement is obtained, including the experimentally observed symmetry characteristics of the phase images. Slight deviations between experiment and numerics are likely due to the approximations of the numerical model, including the absence of the substrate, the approximation of the nanoparticles shape as ideal cylinders, the assumption of plane-wave excitation, and the extraction of the near-fields in a specified plane. The numerical field enhancement at the center of the hot spots is about twice the incident field amplitude for the out-of-plane E_z component. We also calculate the near-field profiles inside the nanodisks as well as the magnetic near-field profiles in order to obtain additional insight into the nature of the observed mode (see Supporting Information).

The numerical simulations furthermore allow us to calculate the scattering and absorption cross sections of the silicon nanodisk. These results are shown in Figure 4a for 60° tilted

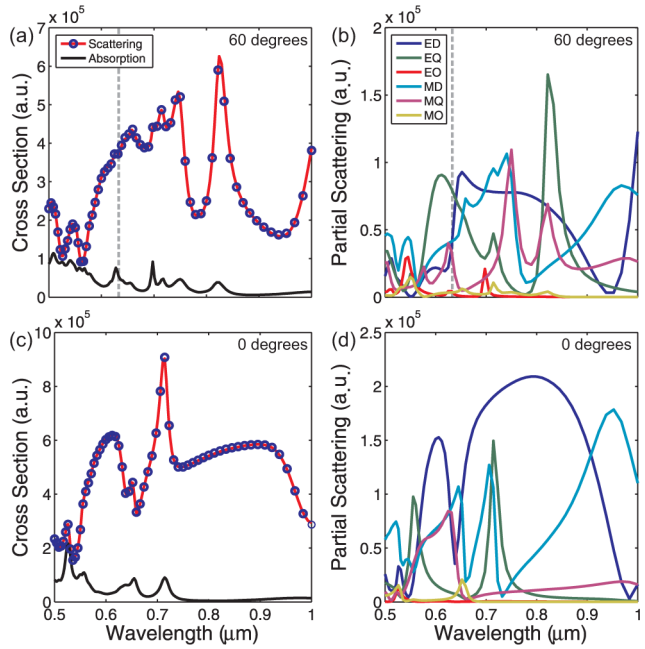

Figure 4. (a) Numerically calculated scattering and absorption cross sections of an individual silicon nanodisk (h = 140, d = 412 nm) in vacuum for 60° incidence of an incident plane wave. (b) Multipolar contributions to the scattering cross section shown in (a) revealed by numerical multipole expansion based on vector spherical harmonics.[29] ED, EQ, and EO (MD, MQ, MO) in the legend stand for electric (magnetic) dipole, quadrupole, and octupole contributions, respectively. (c, d) Corresponding data for normal incidence.

incidence of the exciting plane wave corresponding to our experimental conditions. However, these results do not provide any information about the specific multipole characteristics of the experimentally observed nanodisk mode. To answer this question, we perform a multipole expansion of the scattered field based on vector spherical harmonics.[29] Naturally, the sum of all multipole contributions, represented by the blue circles in Figure 4a, coincides with the scattering cross section obtained from the simulations. Figure 4b shows the scattering cross section decomposed into its electric and magnetic multipole contributions. In order to obtain the contribution of one specific multipole, we sum over scattering into all spherical harmonics that have the same multipole order. The analysis confirms that for 60° incidence, the electric quadrupole (EQ) contribution to the extinction cross section of the silicon nanodisk is dominant at 633 nm. Nevertheless, there are

dx.doi.org/10.1021/ph500232u | ACS Photonics 2014, 1, 794–798

additional non-negligible contributions from the electric dipole (ED), the magnetic dipole (MD), and the magnetic quadrupole (MQ). Figure 4c,d shows corresponding results for normal incidence. Note that the electric quadrupole contribution becomes very small in this case, indicating that tilted incidence is crucial for efficient excitation of the quadrupolar-dominated mode at 633 nm wavelength.

In conclusion, we have presented the first optical near-field measurements of localized modes of high-index all-dielectric nanoparticles. We directly confirm the existence of multiple subwavelength hot-spots with defined phase relations at the surface of subwavelength silicon nanodisks for the investigated electric quadrupole dominated mode. Our results provide valuable input for the design of highly efficient all-dielectric nanoantennas for directional and complex-polarization controlled emission. They may furthermore open a route toward low-loss feed elements for coupling to higher-order optical transitions and for nanoparticle-mediated coherent coupling of multiple emitters.

METHODS

Fabrication. Silicon nanodisks on silicon oxide substrate have been fabricated using electron-beam lithography on silicon-on-insulator wafers (SOITEC, 220 nm top silicon thickness, 2 μm buried oxide thickness) using the negative-tone resist NEB-31A and HMDS as adhesion promoter. We have reduced the initial thickness of the top silicon layer from 220 to 140 nm by interferometrically in situ monitored reactive ion etching before the exposure. After exposure, a second reactive ion etching step has been performed for lateral patterning of the resulting silicon layer using the electron-beam resist pattern as an etch mask. Great care has been taken to remove all residual resist after reactive ion etching by oxygen plasma and piranha etching in order to ensure efficient coupling of the probe tip to the optical modes of the silicon nanodisks. The success of the resist removal has been confirmed by topography measurements (see Figure 2d) in the same ANSOM system used for the near-field optical measurements.

Near-Field Measurements. Polarization selective ANSOM imaging has been performed by configuring the optical components around a Neaspec atomic force microscope customized for pseudoheterodyne interferometric detection of scattered light.[19] A linearly polarized laser beam is focused at a PtIr coated silicon probe tip using a parabolic mirror (NA = 0.46), which is situated to result in an incidence angle of 60° with respect to the sample surface normal. The laser beam is x-polarized, as defined in Figure 1. The scattered light is collected through the same parabolic mirror and mixed with a reference beam. Polarization selection of the scattered light is achieved by controlling the polarization of the reference beam using a quarter waveplate. The polarization selection is further refined using a polarizer mounted close to the detector. The AFM is operated in tapping mode with a tapping amplitude of 45−50 nm near the resonance oscillation frequency $\Omega \approx 250$ kHz of the cantilever. The scattered light plus the reference beam is detected using a silicon photodiode. The output of the detector is demodulated at 4Ω. E_x and E_z refer to the in-plane and out-of-plane near-field vector components, respectively, as shown in Figure 1.

Numerical Simulations. Numerical simulations are performed using the frequency-domain solver of the commercial software package CST Microwave Studio. The nanodisks have been modeled using dispersive optical silicon from the CST material database. We use plane wave excitation and open boundary conditions. The nanodisk is tilted with respect to the computational cell in order to take the incidence angle of 60° into account.

ASSOCIATED CONTENT

Supporting Information

Near-field images demonstrating the reproducibility of our measurements on a different nanodisk sample (Figure S1) and for a different experiment using a different probe (Figure S2); Numerical calculation of magnetic near-field profiles and near-fields inside the nanodisks (Figure S3). This material is available free of charge via the Internet at http://pubs.acs.org.

AUTHOR INFORMATION

Corresponding Authors

*E-mail: habteyes@unm.edu.

*E-mail: isabelle.staude@anu.edu.au.

Author Contributions

†These authors contributed equally to this work (T.G.H. and I.S.).

Notes

The authors declare no competing financial interest.

ACKNOWLEDGMENTS

This work was performed, in part, at the Center for Integrated Nanotechnologies, an Office of Science User Facility operated for the U.S. Department of Energy (DOE) Office of Science. Sandia National Laboratories is a multiprogram laboratory managed and operated by Sandia Corporation, a wholly owned subsidiary of Lockheed Martin Corporation, for the U.S. Department of Energy's National Nuclear Security Administration under contract DE-AC04-94AL85000. The authors also acknowledge a support from the Australian Research Council.

REFERENCES

(1) Bohren, C. F.; Huffman, D. R. *Absorption and Scattering of Light by Small Particles*; Wiley-Interscience: New York, 1983.

(2) Evlyukhin, A. B.; Novikov, S. M.; Zywietz, U.; Eriksen, R. L.; Reinhardt, C.; Bozhevolnyi, S. I.; Chichkov, B. N. Demonstration of Magnetic Dipole Resonances of Dielectric Nanospheres in the Visible Region. *Nano Lett.* **2012**, *12*, 3749−3755.

(3) Kuznetsov, A. I.; Miroshnichenko, A. E.; Fu, Y. H.; Zhang, J.; Luk'yanchuk, B. Magnetic Light. *Sci. Rep.* **2012**, *2*, 492−1−492−6.

(4) Ginn, J. C.; Brener, I.; Peters, D. W.; Wendt, J. R.; Stevens, J. O.; Hines, P. F.; Basilio, L. I.; Warne, L. K.; Ihlefeld, J. F.; Clem, P. G.; Sinclair, M. B. Realizing Optical Magnetism from Dielectric Metamaterials. *Phys. Rev. Lett.* **2012**, *108*, 097402−1−097402−5.

(5) Fu, Y. H.; Kuznetsov, A. I.; Miroshnichenko, A. E.; Yu, Y. F.; Luk'yanchuk, B. Directional Visible Light Scattering by Silicon Nanoparticles. *Nat. Commun.* **2013**, *4*, 1527−1−1527−6.

(6) Staude, I.; Miroshnichenko, A. E.; Decker, M.; Fofang, N. T.; Liu, S.; Gonzales, E.; Dominguez, J.; Luk, T. S.; Neshev, D. N.; Brener, I.; Kivshar, Yu. S. Tailoring Directional Scattering through Magnetic and Electric Resonances in Subwavelength Silicon Nanodisks. *ACS Nano* **2013**, *7*, 7824−7832.

(7) Evlyukhin, A. B.; Eriksen, R. L.; Cheng, W.; Beermann, J.; Reinhardt, C.; Petrov, A.; Prorok, S.; Eich, M.; Chichkov, B. N.; Bozhevolnyi, S. I. Optical Spectroscopy of Single Si Nanocylinders with Magnetic and Electric Resonances. *Sci. Rep.* **2014**, *4*, 4126−1−4126−7.

(8) Person, S.; Jain, M.; Lapin, Z.; Sáenz, J. J.; Wicks, G.; Novotny, L. Demonstration of Zero Optical Backscattering from Single Nanoparticles. *Nano Lett.* **2013**, *13*, 1806−1809.

(9) Krasnok, A. E.; Simovski, C. R.; Belov, P. A.; Kivshar, Yu. S. Superdirective Dielectric Nanoantennas. *Nanoscale* **2014**, *6*, 7354−7361.
(10) Wu, C.; Arju, N.; Kelp, G.; Fan, J. A.; Dominguez, J.; Gonzales, E.; Tutuc, E.; Brener, I.; Shvets, G. Spectrally Selective Chiral Silicon Metasurfaces Based on Infrared Fano Resonances. *Nat. Comm.* **2014**, *5*, 3892-1−3892-9.
(11) Chong, K. E.; Hopkins, B.; Staude, I.; Miroshnichenko, A. E.; Dominguez, J.; Decker, M.; Neshev, D. N.; Brener, I.; Kivshar, Yu. S. Observation of Fano Resonances in All-Dielectric Nanoparticle Oligomers. *Small* **2014**, *10*, 1985−1990.
(12) Hancu, I. M.; Curto, A. G.; Castro-López, M.; Kuttge, M.; van Hulst, N. F. Multipolar Interference for Directed Light Emission. *Nano Lett.* **2014**, *14*, 166−171.
(13) Kruk, S. S.; Decker, M.; Staude, I.; Schlecht, S.; Greppmair, M.; Neshev, D. N.; Kivshar, Yu. S. Spin Polarized Light Emission from Quantum Dots Coupled to Multipolar Nanoantennas, in CLEO:QELS Fundamental Science. *OSA Technical Digest Paper: FF2K.1*; Optical Society of America: Washington, DC, 2014.
(14) Gómez, D. E.; Vernon, K. C.; Mulvaney, P.; Davis, T. J. Surface Plasmon Mediated Strong ExcitonPhoton Coupling in Semiconductor Nanocrystals. *Nano Lett.* **2009**, *10*, 274−278.
(15) Coenen, T.; Van de Groep, J.; Polman, A. Resonant Modes of Single Silicon Nanocavities Excited by Electron Irradiation. *ACS Nano* **2013**, *7*, 1689−1698.
(16) Kiesow, K. I.; Dhuey, S.; Habteyes, T. G. Mapping near-Field Localization in Plasmonic Optical Nanoantennas with 10 nm Spatial Resolution. *Appl. Phys. Lett.* **2014**, *105*, 053105−1−053105−5.
(17) Zenhausern, F.; Oboyle, M. P.; Wickramasinghe, H. K. Apertureless near-Field Optical Microscope. *Appl. Phys. Lett.* **1994**, *65*, 1623−1625.
(18) Inouye, Y.; Kawata, S. Near-Field Scanning Optical Microscope with a Metallic Probe Tip. *Opt. Lett.* **1994**, *19*, 159−161.
(19) Habteyes, T. G.; Dhuey, S.; Kiesow, K. I.; Vold, A. Probe-Sample Optical Interaction: Size and Wavelength Dependence in Localized Plasmon near-Field Imaging. *Opt. Exp.* **2013**, *21*, 21607−21617.
(20) Esteban, R.; Vogelgesang, R.; Dorfmüller, J.; Dmitriev, A.; Rockstuhl, C.; Etrich, C.; Kern, K. Direct near-Field Optical Imaging of Higher Order Plasmonic Resonances. *Nano Lett.* **2008**, *8*, 3155−3159.
(21) Jones, A. C.; Olmon, R. L.; Skrabalak, S. E.; Wiley, B. J.; Xia, Y. N.; Raschke, M. B. Mid-IR Plasmonics: Near-Field Imaging of Coherent Plasmon Modes of Silver Nanowires. *Nano Lett.* **2009**, *9*, 2553−2558.
(22) Schnell, M.; García-Etxarri, A.; Huber, A. J.; Crozier, K.; Aizpurua, J.; Hillenbrand, R. Controlling the near-Field Oscillations of Loaded Plasmonic Nanoantennas. *Nat. Photonics* **2009**, *3*, 287−291.
(23) Alonso-Gonzalez, P.; Schnell, M.; Sarriugarte, P.; Sobhani, H.; Wu, C.; Arju, N.; Khanikaev, A.; Golmar, F.; Albella, P.; Arzubiaga, L.; Casanova, F.; Hueso, L. E.; Nordlander, P.; Shvets, G.; Hillenbrand, R. Real-Space Mapping of Fano Interference in Plasmonic Metamolecules. *Nano Lett.* **2011**, *11*, 3922−3926.
(24) Dorfmüller, J.; Dregely, D.; Esslinger, M.; Khunsin, W.; Vogelgesang, R.; Kern, K.; Giessen, H. Near-Field Dynamics of Optical Yagi-Uda Nanoantennas. *Nano Lett.* **2011**, *11*, 2819−2824.
(25) Knoll, B.; Keilmann, F. Enhanced Dielectric Contrast in Scattering-Type Scanning near-Field Optical Microscopy. *Opt. Commun.* **2000**, *182*, 321−328.
(26) Hillenbrand, R.; Knoll, B.; Keilmann, F. Pure Optical Contrast in Scattering-Type Scanning near-Field Microscopy. *J. Microsc. (Oxford, U. K.)* **2001**, *202*, 77−83.
(27) Kim, Z. H.; Liu, B.; Leone, S. R. Nanometer-Scale Optical Imaging of Epitaxially Grown GaN and InN Islands Using Apertureless near-Field Microscopy. *J. Phys. Chem. B* **2005**, *109*, 8503−8508.
(28) Kim, Z. H.; Ahn, S. H.; Liu, B.; Leone, S. R. Nanometer-Scale Dielectric Imaging of Semiconductor Nanoparticles: Size-Dependent Dipolar Coupling and Contrast Reversal. *Nano Lett.* **2007**, *7*, 2258−2262.
(29) Grahn, P.; Shevchenko, A.; Kaivola, M. Electromagnetic Multipole Theory for Optical Nanomaterials. *New J. Phys.* **2012**, *14*, 093033−1−093033−11.